Biomedical Physics & Engineering Express

PAPER

Synthesis, physicochemical characteristics, cytocompatibility, and antibacterial properties of iron-doped biphasic calcium phosphate nanoparticles with incorporation of silver

RECEIVED
3 June 2023

REVISED
25 July 2023

ACCEPTED FOR PUBLICATION
25 September 2023

PUBLISHED
11 October 2023

Lei Nie[1,2,8,*], **Pengbo Chang**[3,8], **Oseweuba Valentine Okoro**[2], **Musa Ayran**[4], **Oguzhan Gunduz**[4], **Kehui Hu**[5,6,*], **Tianwen Wang**[7] **and Amin Shavandi**[2]

[1] College of Life Sciences, Xinyang Normal University (XYNU), Xinyang 464000, People's Republic of China
[2] Université libre de Bruxelles (ULB), École polytechnique de Bruxelles - BioMatter unit, Avenue F.D. Roosevelt, 50 - CP 165/61, 1050 Brussels, Belgium
[3] Department of Materials Engineering, Zhengzhou Technical College, Zhengzhou 450121, People's Republic of China
[4] Center for Nanotechnology and Biomaterials Application & Research (NBUAM), Marmara University, Istanbul, Turkey
[5] State Key Laboratory of Tribology, Tsinghua University, Beijing 100084, People's Republic of China
[6] Department of Mechanical Engineering, Tsinghua University, Beijing 100084, People's Republic of China
[7] College of Biology and Food Engineering, Anhui Polytechnic University, Wuhu 241000, Anhui, People's Republic of China
[8] These authors contributed equally to this work and should be considered co-first authors.
[*] Authors to whom any correspondence should be addressed.

E-mail: nieleifu@yahoo.com, nielei@xynu.edu.cn **and** hukehui@tsinghua.edu.cn

Keywords: biphasic calcium phosphate, silver nanoparticles, iron, antibacterial activity, biocompatibility

Abstract

The application of biphasic calcium phosphate (BCP) in tissue engineering and regenerative medicine has been widely explored due to its extensively documented multi-functionality. The present study attempts to synthesize a new type of BCP nanoparticles, characterised with favourable cytocompatibility and antibacterial properties via modifications in their structure, functionality and assemblage, using dopants. In this regard, this study initially synthesized iron-doped BCP (FB) nanoparticles with silver subsequently incorporated into FB nanoparticles to create a nanostructured composite (FB_{Ag}). The FB and FB_{Ag} nanoparticles were then characterized using Fourier transform infrared spectroscopy, x-ray diffraction, ultraviolet-visible spectroscopy, and x-ray photoelectron spectroscopy. The results showed that silver was present in the FB_{Ag} nanoparticles, with a positive correlation observed between increasing $AgNO_3$ concentrations and increasing shape irregularity and reduced particle size distribution. Additionally, cell culture tests revealed that both FB and FB_{Ag} nanoparticles were compatible with bone marrow-derived mesenchymal stem cells (hBMSCs). The antibacterial activity of the FB_{Ag} nanoparticles was also tested using Gram-negative *E. coli* and Gram-positive *S. aureus*, and was found to be effective against both bacteria. The inhibition rates of FB_{Ag} nanoparticles against *E. coli* and *S. aureus* were 33.78 ± 1.69–$59.03 \pm 2.95\%$, and 68.48 ± 4.11–$89.09 \pm 5.35\%$, respectively. These findings suggest that the FB_{Ag} nanoparticles have potential use in future biomedical applications.

1. Introduction

Tissue engineering is widely used in tissue grafting applications due to the high number of patients who require grafting due to congenital conditions, trauma, and tumour resection [1–3]. Tissues such as bone, tooth enamel, dentin, and cementum, contain significant amounts of ionic substitutions, including sodium, potassium, and carbonate groups, which can affect the functionality of related tissues. Calcium phosphate (CaP) nanoparticles, such as hydroxyapatite (HA), β-tricalcium phosphate (β-TCP), tetra calcium phosphate (TTCP), biphasic calcium phosphate (BCP), are commonly used in bone tissue engineering due to their excellent biocompatibility, biodegradability, and adjustable physicochemical properties [2, 4, 5]. Especially, BCP, composed of HA and β-TCP, has been shown to have favourable

properties (i.e., biological activity and adjustable degradation rate) in bone regeneration [6–8].

Notably, although BCP has several favourable properties, its mechanical properties, osteoinductivity, cytocompatibility, and osteoconductivity properties need to be further enhanced to be efficiently employed in artificial bone repair [4]. Indeed, improving the above properties will help to ensure that complex tissue repair and regeneration occur more efficiently. It is also crucial that the BCP possesses inherent antibacterial properties since there is a risk of infections due to exposure to contaminated implanted medical devices or scaffolds, leading to biofilm formation and localized inflammation issues [9]. Therefore, scaffolds with excellent antibacterial properties provide a significant advantage in the clinical stage.

Many metal nanoparticles, such as silver (Ag), zinc oxide (ZnO), and titanium dioxide (TiO_2), have strong antibacterial properties and low toxicity toward mammalian cells and have been widely applied in a range of areas [2, 10–12]. For instance, Li *et al* [13,] prepared porous silver-incorporated calcium phosphate nanocomposites to make them possess antibacterial functions for active antibacterial bioprotective mask applications. Varun *et al* [14,] also synthesized Ag-BCP microclusters with excellent antibacterial activity using the double emulsion method. Iron (Fe) is an essential trace element that plays a vital role in bone metabolism and is found in high concentrations in human bone tissue [15, 16]. Iron is also essential for functioning enzymes and cytochromes and helps regulate various physiological processes. Studies have shown that bone density increases when the iron content in their environment is higher and decreases when the iron intake from food is reduced, which leads to bone fragility and increases the risk of osteoporosis [17, 18]. Insufficient iron intake also affects the differentiation and mineralization of osteoblasts and the synthesis of collagen fibers, which are necessary for mineralization [17, 19]. Iron also affects collagen synthesis and vitamin D metabolism, and abnormal iron concentrations can affect osteoblast activity and cause abnormal bone metabolism [20, 21]. It is therefore implied that iron plays a role in bone regeneration by influencing the synthesis of collagen fibers [15].

The death of the bacteria is because the binding with the RNA and DNA leads to their condensation, thus making their transcription (i.e. crucial for protein synthesis and cell proliferation) by ribosomes difficult [22]. The antibacterial effect of nanoparticles can be influenced by size, shape, nanostructure, and chemical modification. Furthermore, it has been reported that the substitution of metal ions in CaP-based nanoparticles also shows powerful antibacterial effects, such as selenium-substituted hydroxyapatite (Se-HA) nanoparticles. We have already shown that Se-HA nanoparticles display excellent biocompatibility and inhibit specific bacterial strains of interest [5]. Silver is also stable in body fluids and can be used in antibacterial implants because its ions can easily bind to bacterial DNA and RNA, resulting in bacteria death [22, 23].

In this study we synthesised nanostructured iron-doped biphasic calcium phosphate nanoparticles with *in situ* incorporated silver via an easy and rapid precipitation method and characterized the physicochemical properties of the nanoparticles. The cytocompatibility of the prepared nanoparticles was also evaluated. Furthermore, the antibacterial activity against Gram-negative *E. coli* and Gram-positive *S. aureus* was also investigated, and the results showed that the prepared nanoparticles had the potential for antibacterial applications in tissue engineering and regenerative medicine (Scheme 1).

2. Materials and methods

2.1. Chemicals

Calcium chloride ($CaCl_2$) and iron (III) chloride hexahydrate ($FeCl_3{\cdot}6H_2O$) were obtained from Kermel Co., Ltd. Ammonium dihydrogen phosphate ($(NH_4)_2HPO_4$), 99.0%) was obtained from Shanghai Macklin Biochemical Co., Ltd. Silver nitrate ($AgNO_3$) was obtained from Tianjin Tiangan Chemical Technology Development Co., Ltd Ammonium solution ($NH_3.H_2O$, 25∼28%) was purchased from Ron Reagent Co., Ltd Millipore water was prepared in the lab (Milli-Q50 SP Reagent Water System, Millipore Corporation, MA, USA). All chemicals used in this paper were analytical grade procured from commercial sources and used as received.

2.2. Synthesis of iron-doped biphasic calcium phosphate (FB) nanoparticles

The FB nanoparticles were synthesized based on methods described in our previous papers with some modifications [24, 25]. First, a mixed solution of $CaCl_2$ and $FeCl_3{\cdot}6H_2O$ (solution A, concentration), and $(NH_4)_2HPO_4$ solution (solution B, concentration) were prepared, respectively. A volume of solution B was added to a 50 ml solution A, in a three-neck flask, to achieve the mole ratios highlighted in table 1 and stirred for 4 h. Then, the pH of the stirred solution was adjusted to 11 using concentration ammonium solution, and stirred continuously for an additional 30 min, with precipitate formation observed. After that, the precipitates were collected and washed thrice using Millipore water. The washed precipitates were then dried to constant mass at 120 °C for 8 h in a vacuum oven to obtain FB nanoparticles. Different FB nanoparticles were synthesized, according to table 1.

2.3. Synthesis of FB nanoparticles incorporated with silver (FBAg)

Next, FB nanoparticle powder was dispersed in 100 ml Millipore water in a three-neck flask, and the $AgNO_3$ was added slowly to the mixture. The mixed solution was stirred for 4 h at room temperature (RT), with the

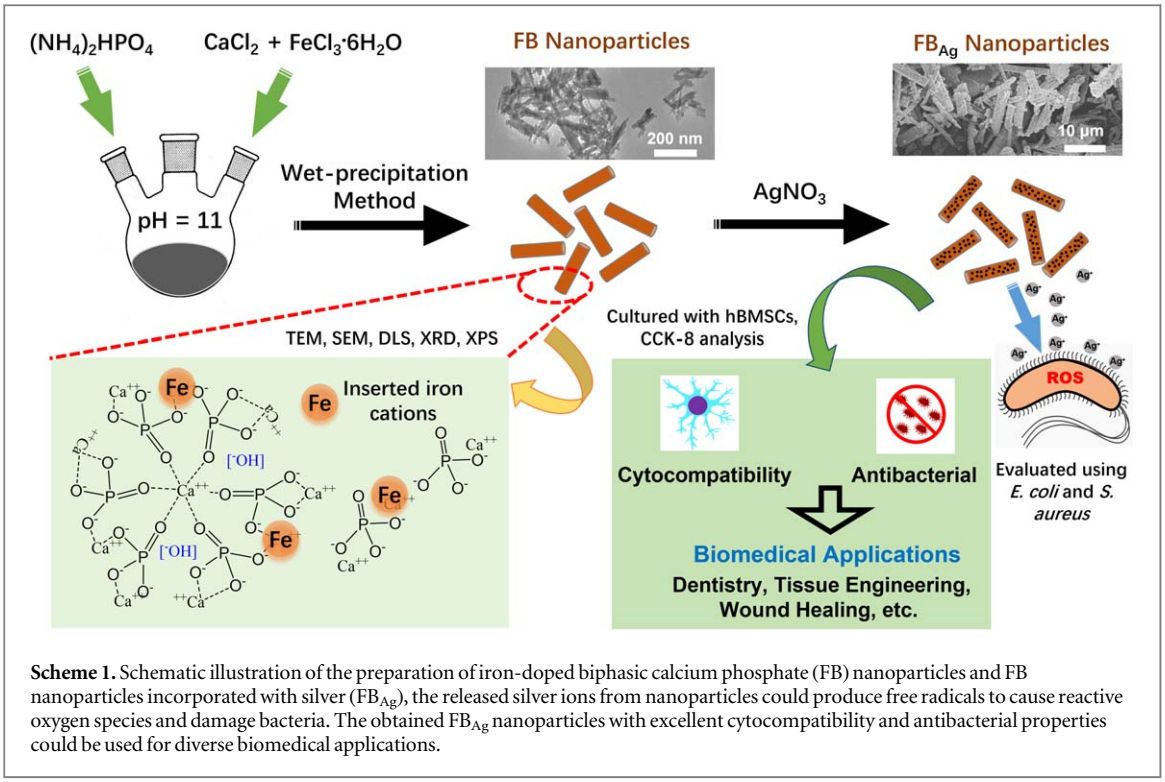

Scheme 1. Schematic illustration of the preparation of iron-doped biphasic calcium phosphate (FB) nanoparticles and FB nanoparticles incorporated with silver (FB_{Ag}), the released silver ions from nanoparticles could produce free radicals to cause reactive oxygen species and damage bacteria. The obtained FB_{Ag} nanoparticles with excellent cytocompatibility and antibacterial properties could be used for diverse biomedical applications.

Table 1. The designation of iron-doped biphasic calcium phosphate (FB) nanoparticle.

Nanoparticles	FB-1	FB-2	FB-3	FB-4	FB-5
(Ca + Fe)/P[a]	1.67	1.67	1.67	1.67	1.67
Ca/Mg[a]	0.05	0.10	0.15	0.20	0.25

[a] Mole ratio.

resultant precipitates collected and subsequently dried to constant mass at 60 °C for 4 h using a vacuum oven. A nanostructured FB_{Ag} was obtained (Scheme 1). Different FB_{Ag} nanoparticles were synthesized by adjusting the mass ratio of FB nanoparticles and $AgNO_3$ (table 2).

2.4. Dynamic light scattering (DLS) analysis

The size distribution of FB and FB_{Ag} nanoparticles in water was examined at 20 °C by Dynamic Light Scattering (DLS, Malvern Zetasizer 3000E). The sample was dispersed in water and sonicated for 1 h, and each measurement was performed in triplicate.

2.5. Transmission electron microscopy (TEM) analysis

Samples of FB and FB_{Ag} nanoparticles were dispersed in ethanol and sonicated for 2 h, and then a copper grid was dipped into the above solutions and dried under an infrared lamp. Transmission Electron Microscopy (TEM, Tecnai G2 F20) was also used to investigate morphologies of FB and FB_{Ag} nanoparticles.

2.6. Scanning electron microscopy (SEM) analysis

The morphologies of FB and FB_{Ag} nanoparticles were also observed with a cold field emission scanning electron microscope (SEM, Hitachi, S-4800). The dried nanoparticles were adhered to the sample table using a conductive glue and then spray coated with a thin Pt conductive layer on its surface before SEM observation.

2.7. Fourier transform infrared spectroscopy (FT-IR) analysis

The specific chemical groups in FB and FB_{Ag} nanoparticles were confirmed using FT-IR (ThermoFisher, Nicolelis5). The sample powders were mixed with KBr, ground, and pressed into thin sections, and the KBr was measured as a blank control. FT-IR spectra were obtained using the SEM at an accelerated voltage, so spectra within the range between 4000 and 500 cm^{-1} were obtained at a spectral resolution of 1 cm^{-1}.

2.8. Ultraviolet-visible spectroscopy (UV–vis) analysis

The diffuse reflectance spectra of FB and FB_{Ag} nanoparticles were investigated using Ultraviolet-visible Spectroscopy (UV–vis, PerkinElmer, Lambda 950), equipped with an integrating sphere attachment. The sample was operated in the 200–800 nm range at 298 K for the optical diffuse reflectance (DRS) spectra.

2.9. X-ray diffraction (XRD) Analysis

Both FB and FB_{Ag} nanoparticles were analyzed by x-ray diffraction (XRD). The tested samples were sprinkled as evenly as possible on the glass slide and

Table 2. The designation of iron-doped biphasic calcium phosphate nanoparticles incorporation of silver (FB_{Ag}).

Nanoparticles	$FB_{Ag}-1$	$FB_{Ag}-2$	$FB_{Ag}-3$	$FB_{Ag}-4$	$FB_{Ag}-5$
$AgNO_3$[a]	30	60	90	120	150
FB nanoparticles[b]	200	200	200	200	200

[a] mg.

[b] sample FB-4 was used for the preparation of FB_{Ag}.

stacked inside the hole of the glass slide. X-ray powder diffraction (XRD) patterns of samples were collected using an x-ray diffractometer (Rigaku Smartlab 9 kW), operating at 45 kV and 200 mA with Cu Kα radiation ($\lambda = 1.5406$ Å) and a spinning sample holder. XRD data were acquired in the 2θ range of 10°–70° at a step increment of 0.05°.

2.10. X-ray photoelectron spectroscopy (XPS) analysis

Both FB and FB_{Ag} nanoparticles were also measured by X-ray Photoelectron Spectroscopy (XPS, K-Alpha 0.05 eV, Thermo Scientific) to obtain their elemental composition. The nanoparticles powder was sprinkled and covered on the tape evenly, the aluminum foil was used to press the sample (around 6 MPa), then the aluminum foil was peeled, and the sample was placed in a clean sealing bag and tested by XPS analyzer.

2.11. CCK-8 assay

The human bone marrow-derived mesenchymal stem cells (hBMSCs, ATCC@PCS-500-012™) were used to evaluate the cytocompatibility of FB and FB_{Ag} nanoparticles. Cells were cultured according to ATCC protocols, and cells at passage five were used for the subsequent experiments. First, a certain amount of FB and FB_{Ag} nanoparticles were added into the cell medium, and no agglomeration phenomenon was not observed under optical microscopy. The final nanoparticle concentrations for testing were adjusted to 100, 250, and 500 $\mu g\ ml^{-1}$. The viabilities of the cells cultured with nanoparticles were quantitatively investigated by the Cell Counting Kit-8 (CCK-8) assay, and the CCK-8 assay was operated according to the CCK-8 Cell Proliferation Assay Kit protocol. Finally, the absorbance at 450 nm was measured by using a microplate reader to quantify the degree of cell proliferation. The cultured cells without adding nanoparticles as the control group.

2.12. Antibacterial activity assay

The antibacterial activities of FB_{Ag} nanoparticles were evaluated using Gram-negative *E. coli* (ATCC 25922) and Gram-positive *S. aureus* (ATCC 6538). The single colony of *E. coli* and *S. aureus* on the Luria Bertani (LB) agar plate were transferred to a liquid LB culture medium by growing at 37 °C overnight to obtain the seed culture. FB_{Ag} nanoparticles were dispersed in ultrapure water (500 $\mu g\ ml^{-1}$), and then 100 μl of the dispersed solution was mixed with 10 ml autoclaved LB medium, after which 5 μl of seed cultures of *E. coli* or *S. aureus* were inoculated into the medium. After culturing for 12 h at 37 °C, the optical densities of the media were measured using a UV–vis spectrophotometer at 600 nm (OD_{600}). *E. coli* and *S. aureus* were cultivated at similar conditions without nanoparticles and used as the control group (CK). The inhibition rate was calculated by the following equation:

$$Inhibition\ Rate\ (\%) = \frac{K_{CK} - K_S}{K_{CK}} \times 100$$

Where K_{CK} and K_S are the absorptions of the control group and sample group, respectively.

The seed culture medium was diluted into fresh LB medium and cultured under 37 °C. When the OD_{600} of the medium reached about 0.6, the broth was diluted to 105 CFU ml^{-1} with sterile 0.9% NaCl solution. After that, the suspension (50 μl) was spread onto a 90 mm-diameter LB agar plate. The wells were then created with a hole puncher with a diameter of 4 mm with 30 μl of the prepared nanoparticle solutions subsequently added to the wells. The plates were then kept in an incubator at 37 °C for 12 h, and the size of each sample's inhibition zone was subsequently recorded. The diameter of the inhibitory halo was measured, and the radius was used in this paper.

2.13. Statistical analysis

The data were expressed as mean ± standard deviation (SD) of three determinations. The statistical package for the social sciences (SPSS) software (IBM SPSS Statistics, Version 22.0) was used for the analysis. The data were analyzed using one-way ANOVA, and a P value < 0.05 was considered statistically significant.

3. Results and discussion

3.1. Physicochemical characterization of FB and FB_{Ag} nanoparticles

Firstly, the size and size distribution of nanoparticles are crucial for understanding their physicochemical characteristics and biological behavior [26]. In order to evaluate the deposits and conduct biological research into the biocompatibility of the produced nanoparticles, testing the homogeneity of the FB and FB_{Ag} suspension was required. DLS test (figures 1(a)–(b)) was carried out to quantify the size of nanoparticles and their dispersion characteristics. The results

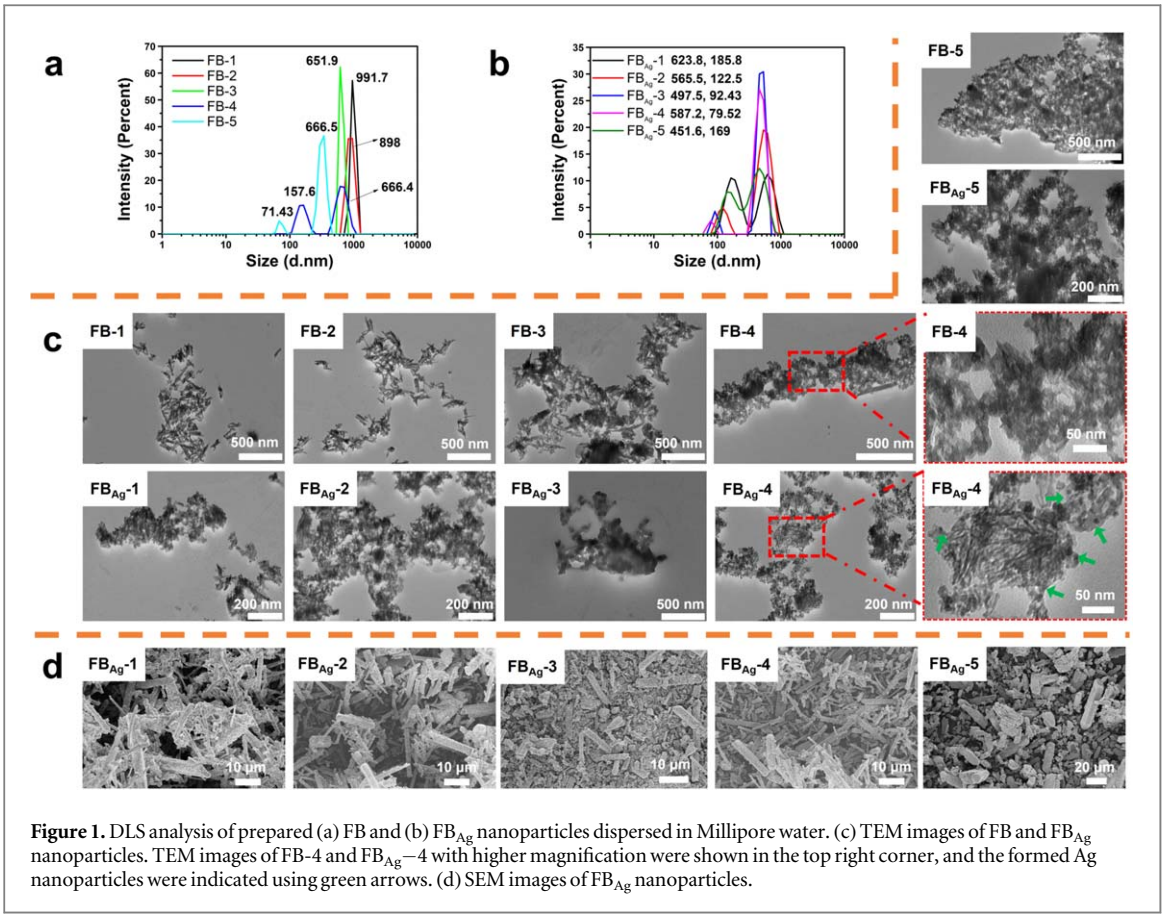

Figure 1. DLS analysis of prepared (a) FB and (b) FB_{Ag} nanoparticles dispersed in Millipore water. (c) TEM images of FB and FB_{Ag} nanoparticles. TEM images of FB-4 and FB_{Ag}−4 with higher magnification were shown in the top right corner, and the formed Ag nanoparticles were indicated using green arrows. (d) SEM images of FB_{Ag} nanoparticles.

showed that increasing hydrodynamic diameters of FB nanoparticles were positively correlated with increasing Ca/Mg molar ratios. However, the size distribution of FB_{Ag} nanoparticles was observed to decrease. For instance, FB-4 and FB-5, which contain higher molar ratios of Ca/Mg in FB nanoparticles, were not monodispersed, indicating that a greater degree of doped nanoparticle agglomeration was present (figure 1(a)). The narrow size distribution of the FB_{Ag} nanoparticles constitutes another finding from this investigation. FB-4 nanoparticles were incorporated with the silver due to the minor hydrodynamic nanoparticle size distribution of FB nanoparticles. The intensity of nanoparticle distribution was observed to reduce by ∼50% when silver was introduced, with a similar trend observed when the sizes of the nanoparticles were observed (figure 1(b)). The samples of FBAg nanoparticles were not monodispersed compared to FB nanoparticles.

The morphologies of FB and FB_{Ag} nanoparticles were also analyzed using TEM, and the TEM images were subsequently displayed in figure 1(c). The nanoparticles from all groups were combined to form large masses at the nanoscale. As the Ca/Mg molar ratio increases, aggregation increases, and the particles randomly condense in the regions. Numerous aggregated nano-sized Ag particles are dispersed throughout the FB nanoparticles, creating a rough surface that can offer increased surface area and, consequently, sufficient sites for cell survival. In addition, the SEM images of the synthesized FB and FB_{Ag} nanoparticles were analysed with their graphs presented in figure 1(d). It was observed that most Ag nanoparticles were typically nanorod-like, indicating that these nanoparticles had a cylindrical shape and were formed when the particles were synthesized. Additionally, agglomerated Ag nanoparticles in FBAg-5 indicate possible sedimentation at higher concentrations. FB_{Ag} also showed irregular morphology, which can be affected by the deposition of the addition of silver. With increased $AgNO_3$ concentration in the FB, it was evident that irregularly shaped particles with a reduced particle size distribution emerged. Furthermore, it was observed that the number of irregular nanorod structures diminished and turned into a complex structure at a high concentration.

FT-IR analysis was undertaken to analyze the functional groups of FB and FB_{Ag} nanoparticles, and the results were subsequently presented in figures 2(a)–(b). It was observed that the prominent peaks of FB nanoparticles were detected at 576 cm^{-1}, and 1016–1030 cm^{-1} can be associated with out-of-plane bending, and asymmetric stretching of phosphate groups (PO_4^{3-}), respectively. The obtained spectra of PO_4^{3-} is expected and consistent with our previous report [2]. The peaks observed at 1648 cm^{-1} and 1436 cm^{-1} indicated the presence of carbonate functionalities in the structure [27]. Notably, the

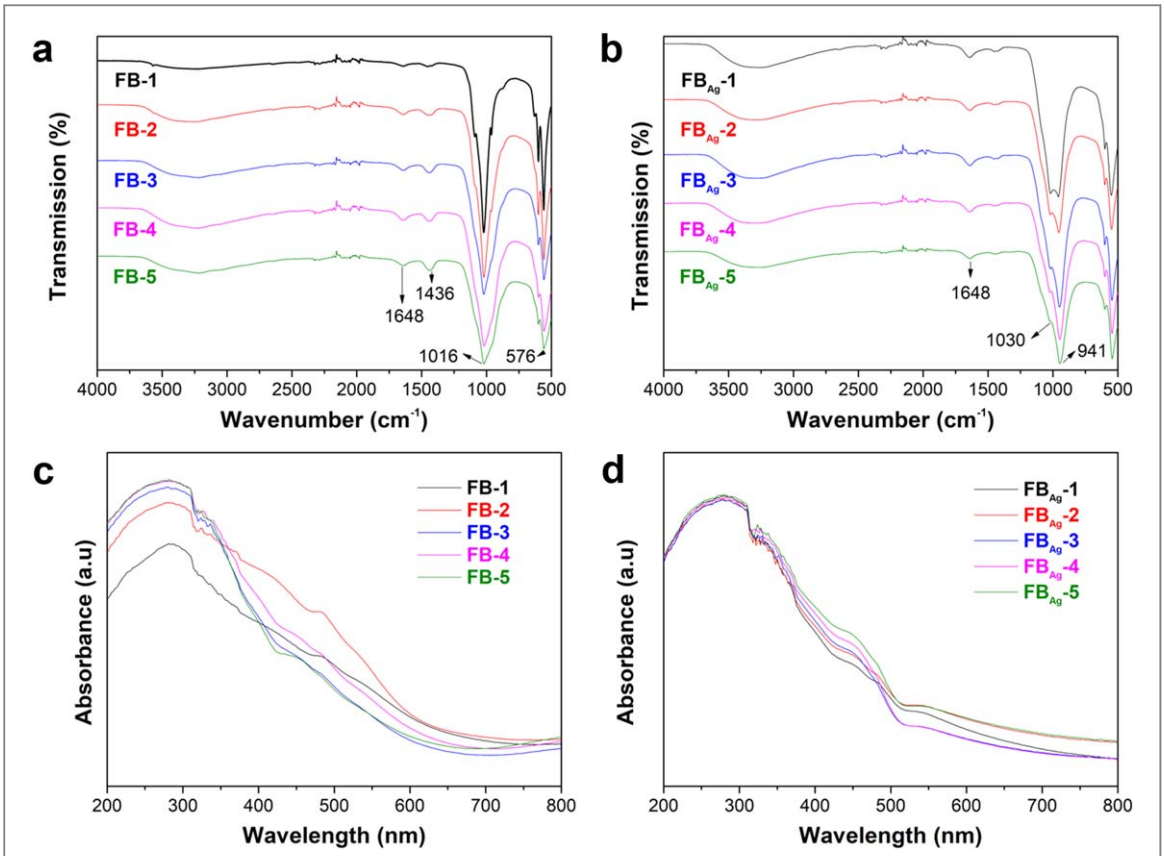

Figure 2. FT-IR spectra of prepared (a) FB and (b) FB_{Ag} nanoparticles. UV–vis DRS spectra of prepared (c) FB and (d) FB_{Ag} nanoparticles.

spectra of the FB and FB_{Ag} nanoparticles were not significantly different from one another, highlighting the similarity of the functional groups present. However, a peak at 941 cm^{-1} was observed in FB_{Ag} nanoparticles only. This peak is due to the stretching vibrations of the PO_4^{3-} with the merging of the two peaks between 940–1030 cm^{-1} observed as the concentration of $AgNO_3$ increases.

As shown in figures 2(c)–(d), the produced FB and FB_{Ag} nanoparticles were examined by UV–vis DRS spectroscopy. The absorbance can change based on many factors, such as particle size, a lack of oxygen, and flaws in the grain structure [28]. The UV–vis DRS absorption expanded in the range of 200–800 nm, with the band at $\lambda = 520$ nm corresponding to the surface plasmon resonance of silver in FB nanoparticles. All nanoparticles were observed to exhibit ultraviolet (UV) absorption with the absorption peak observed at $\lambda = 340$ nm. The UV absorption intensity is especially noticeable in the most doped nanoparticles in FB. The absorption peak at $\lambda = 340$ nm in the UV–vis spectra of a material can be attributed to the $\pi \rightarrow \pi^*$ transition of C=O functional groups [29], which is a characteristic band of carbonyl compounds. Additionally, it is essential to note that FB_{Ag} nanoparticles exhibited a slight absorption in the visible region (400–800 nm). This absorption may be useful in biomedical applications because it can be advantageous to extend the optical activation of the nanoparticles, such as photosensitizing agents in photodynamic therapies [30, 31].

XRD analyses determined the crystalline phase of nanoparticles, and their XRD patterns were displayed in figures 3(a)–(b). The peaks of HA and β-TCP were detected in FB nanoparticles, while the peaks of HA, β-TCP, and Ag were detected in FB_{Ag} nanoparticles. Evident diffraction peaks of FB nanoparticles in XRD patterns can be related to the (0 0 2), (1 0 2), (2 1 1), (3 1 0), (2 2 2), and (2 1 3) planes which are consistent with the typical XRD spectrum of HA (JCPDS No. 9-0432) [32, 33]. The peaks in the (3 3 −2), (1 0 10), (2 1 10), and (3 1 0) are consistent with the standard XRD spectrum of β-TCP (JCPDS, No. 9-0169) [34, 35]. Additionally, the broadening of reflection peaks in XRD patterns for FB nanoparticles indicates the decrease in crystallinity as the Ca/Mg molar ratio increases.

All FB_{Ag} nanoparticles indicated the face-centered cubic crystal structure of silver [36, 37], which matched the peaks that correspond well with (1 1 1), (2 0 0), and (2 2 0) planes and compared with the standard powder diffraction card of JCPDS, silver file No. 87-0720. The theta value corresponding to the (111) plane in FB_{Ag} nanoparticles had the most dramatic peak among the silver peaks. The HA, β-TCP, and Ag peaks overlapped in the XRD pattern for FB_{Ag} nanoparticles, indicating that each component interacted with the others. It can be stated that

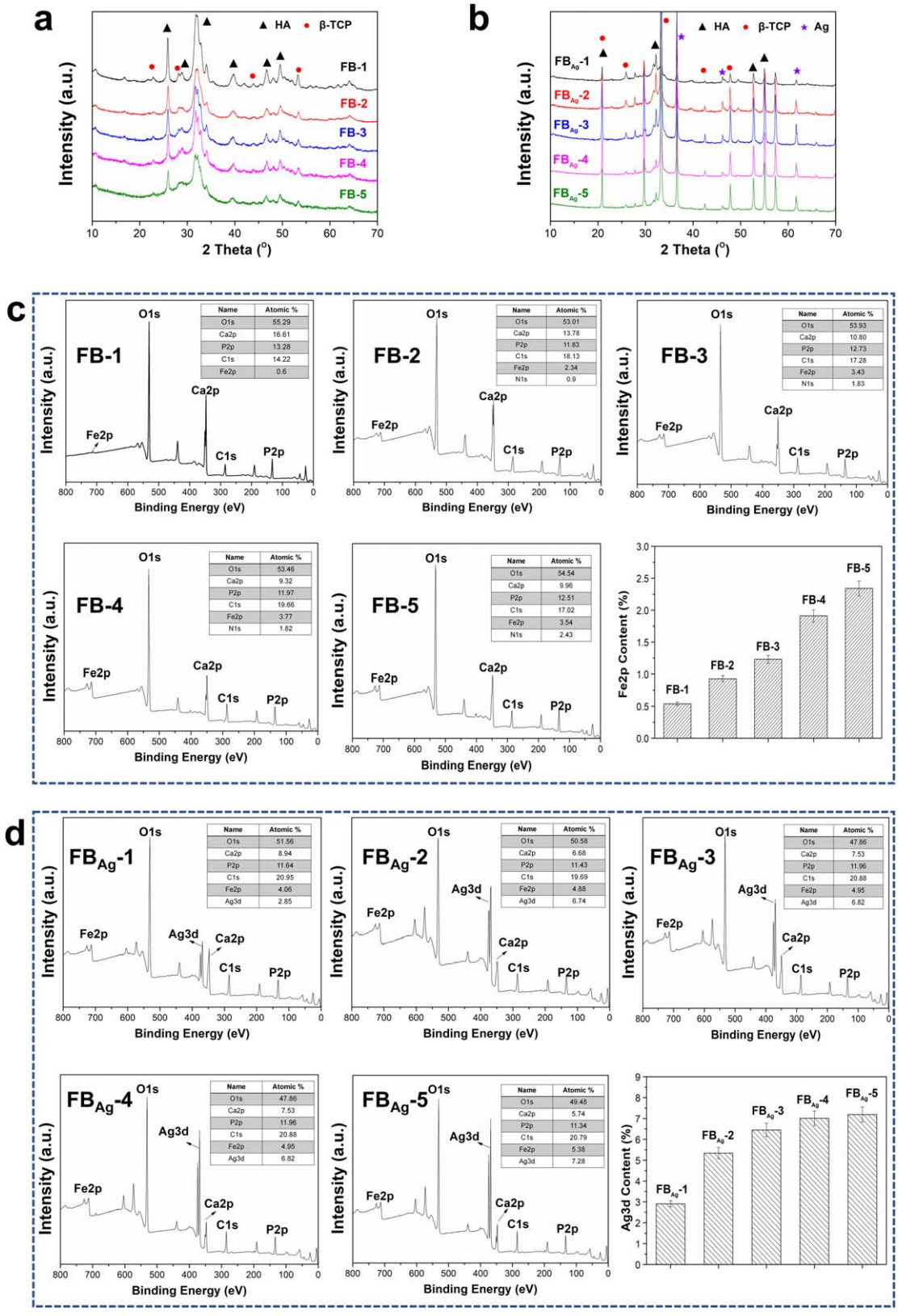

Figure 3. XRD spectra of prepared (a) FB and (b) FB_{Ag} nanoparticles. (c) XPS spectra of prepared FB nanoparticles, and Fe2p content for each FB sample were displayed according to XPS results. (d) XPS spectra of prepared FB_{Ag} nanoparticles, and Ag3d content for each FB_{Ag} sample were displayed according to XPS results.

additional $AgNO_3$-related crystalline phases in FB_{Ag} nanoparticles induced sharper, and broad peaks in all planes except for the (211) plane.

XPS provided more details on the combination and integration of the produced nanoparticles. O, Ca, P, C, N, and Fe were found in the FB nano-

particles according to the extensive energy range analysis (figure 3(c)). A small quantity of observed N in FB nanoparticles was mainly due to the addition of $(NH_4)_2HPO_4$ and ammonium solution during the synthesis process. Regarding the FB_{Ag} nanoparticles, O, Ca, P, C, Fe, and Ag were found in figure 3(d). With the addition of silver in FB nanoparticles, N was not detected anymore. The Ag3d signal at 368 eV ($Ag3d_{5/2}$) and 373 eV ($Ag3d_{3/2}$) showed that the $AgNO_3$ group had already been integrated into the iron-doped BCP lattice [2, 38]. A peak at 132 eV was seen in the P2p spectra of all nanoparticles, which was attributed to the phosphate group. Fe2p has several peaks that break into two distinct components, $Fe2p_{3/2}$ and $Fe2p_{1/2}$, located at around 712 and 723 eV, respectively [39]. Results from XPS and XRD demonstrate the coexistence of both silver cations (Ag^+) and nitrate anions (NO^{3-}) substituting at FB nanoparticles. The dominant Fe valence state (Fe^{2+} or Fe^{3+}) changes in accordance with the total amount of dopant, and it is also observed. They also confirm that the incorporation the Fe dopant within the BCP structure was successful.

3.2. Cytocompatibility of FB and FB_{Ag} nanoparticles

As for the cytocompatibility evaluation of FB and FB_{Ag} nanoparticles, CCK-8 assay was used to measure the cell viability and proliferation after culturing human bone marrow-derived mesenchymal cells (hBMSCs) with nanoparticles for up to 1, 3, and 5 days for confirming their potential biomedical applications, and the cells cultured without adding nanoparticles as the control group. All nanoparticles showed an increase in the number of viable cells over days, suggesting the produced nanoparticles are cytocompatible (figure 4). Notably, as the concentration of the nanoparticles increased from 100 μg ml^{-1} to 500 μg ml^{-1}, O.D values at 450 nm decreased, indicating the decrease in cell number. The addition of $AgNO_3$ into the FB nanoparticles demonstrated a slight decrease in the cell viability of FB_{Ag} nanoparticles. This observation is because the literature has reported the potential of $AgNO_3$ that can harm cell membranes and interfere with cellular metabolism when present in high doses [40–42]. Indeed, in these studies, the researchers found that exposure to $AgNO_3$ reduced cell viability in a dose-dependent manner. Contrary to previous studies, we observed that although cell viability was reduced, the number of viable cells cultured with FB_{Ag} nanoparticles increased over days, highlighting their cytocompatibility.

3.3. Antibacterial activity of FB and FB_{Ag} nanoparticles

In this study, the antibacterial activity of obtained FB and FB_{Ag} nanoparticles was tested using the Agar-well diffusion method and liquid cultured bacteria supplemented with nanoparticles, which worked well to assess the antibacterial activity [43], against both Gram-positive *E. coli* and Gram-negative *S. aureus* strains. Figure 5 illustrates that FB_{Ag} nanoparticles displayed antibacterial activity even at low concentrations of $AgNO_3$ compared to FB nanoparticles. The distinct bacteriostatic halos surrounding FB_{Ag} nanoparticles were observed in disk diffusion against *E. coli* and *S. aureus*. However, bacteriostatic halos surrounding FB nanoparticles were not observed (figures 5(a)–(b)). The inhibition rates of FB and FB_{Ag} nanoparticles against *E. coli* and *S. aureus* for 12 h were calculated, as shown in figures 5(c)–(d). The inhibition rates of FB_{Ag} nanoparticles against *E. coli* and *S. aureus* were 33.78 ± 1.69–59.03 ± 2.95%, and 68.48 ± 4.11–89.09 ± 5.35%, respectively, which were remarkably higher than that of FB nanoparticles against *E. coli* (9.56 ± 0.29–13.63 ± 0.41%) and *S. aureus* (14.87 ± 0.59–16.13 ± 0.65%). Figures 5(e)–(f) show larger, more distinct bacteriostatic halos surrounding FB_{Ag} nanoparticles, indicating excellent inhibitory effects against *E. coli* and *S. aureus* with inhibitory zones larger than 1.2 mm. Further evidence that FB_{Ag} nanoparticles had a more efficient antibacterial effect against *S. aureus* than *E. coli* was illustrated by the lower zone inhibition of *S. aureus* after FB_{Ag} nanoparticles were introduced, compared to the zone inhibition of *E. coli*. In addition, the antibacterial effect could be revealed using bacterial suspension supplemented with nanoparticles after 12 h growth. The bacterial suspension with FB_{Ag} nanoparticles ($FB_{Ag}-1$) in the tube shows transparent liquids compared to FB nanoparticles (FB-1)-added bacterial suspension. Similar antimicrobial activity of silver nanoparticles against *E. coli* and *S. aureus* was reported, and they successfully inhibited bacterial growth [44]. The antimicrobial agent most frequently used is silver. It interacts with proteins' thiolic (-SH) groups to form S-Ag bonds, which render proteins inactive [45]. Moreover, at higher $AgNO_3$ concentrations, the zone inhibition of FB_{Ag} was not noticeably changed, implying that the antibacterial behavior was not dose-dependent. Furthermore, the OD_{600} (figure 5(g)) values showed that *S. aureus* bacteria were not observed after 12 h, when all FB_{Ag} nanoparticles, of varying compositions, were introduced. On the other hand, some *E. coli* bacteria were retained and survived in the culture, after 12 h, in the FB_{Ag} nanoparticles. This observation indicated that FB_{Ag} nanoparticles constituted a more potent bactericidal agent against *S. aureus* compared to *E. coli.* Regarding that, the antibacterial ability of FB_{Ag} nanoparticles was increased with the increased content deposition of silver, which might be due to the fact that more silver nanoparticles were released from FB_{Ag} nanoparticles, which could prevent the adhesion and growth of bacteria. Song *et al*, proved that the silver ions

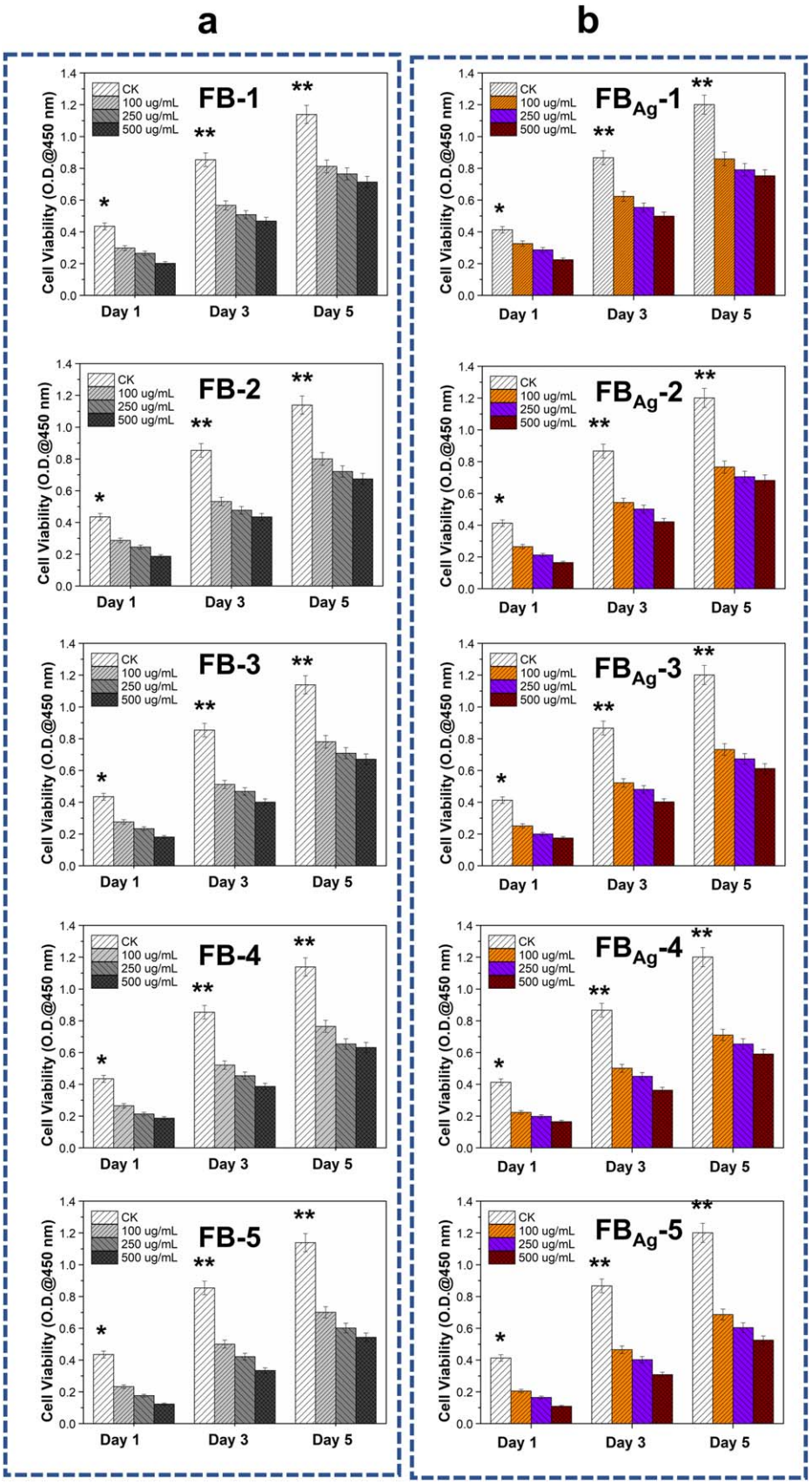

Figure 4. The cytocompatibility of prepared (a) FB and (b) FB_{Ag} nanoparticles was evaluated using CCK-8 after culturing with hBMSCs for 1, 3, and 5 days, and cells cultured without adding nanoparticles as a control group (CK). $^{*}p < 0.05$, $^{**}p < 0.01$.

near the surface of the bacterium could produce free radicals, and generate more reactive oxygen species (ROS), which lead to the damage of bacteria membrane, and bacterial lipase, and induce leaking of the intracellular contents of bacteria until bacterial death [46]. The synthesized FB_{Ag} nanoparticles

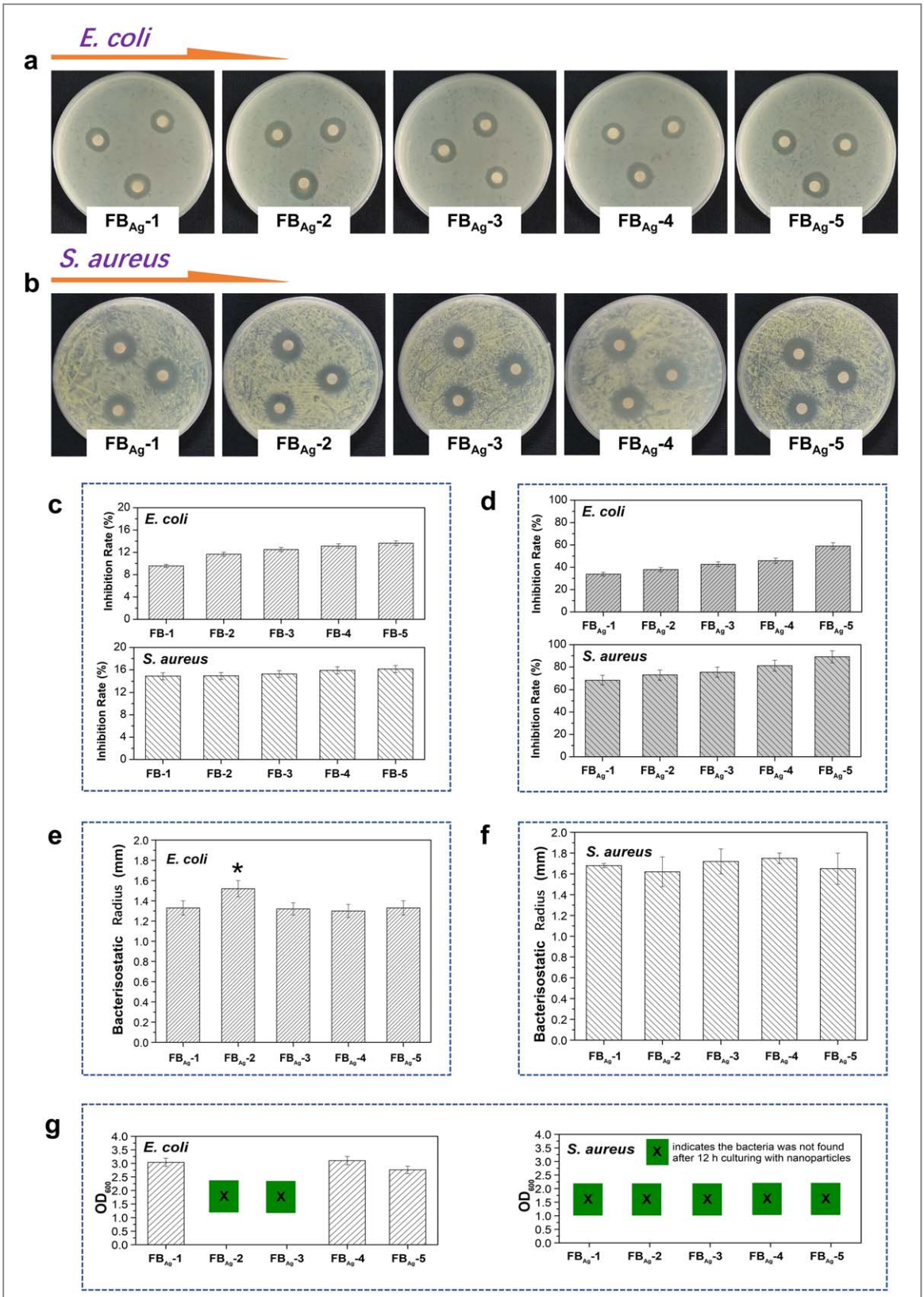

Figure 5. Photos of (a) *E. coli* and (b) *S. aureus* grew on nutrient agar LB plates after the addition of FB_{Ag} nanoparticles for 12 h. Inhibition rate of (c) FB nanoparticles and (d) FB_{Ag} nanoparticles treated on *E. coli* and *S. aureus* for 12 h. Bacteriostatic radius, as inhibitory halo, of (e) *E. coli*, (f) *S. aureus* after adding FB_{Ag} nanoparticles for 12 h, $^{*}p < 0.05$, the radius tested from photos of (a), (b). (g) Optical density at 600 nm (OD_{600}) of *E. coli* and *S. aureus* in the LB medium after 12 h supplemented with FB_{Ag} nanoparticles, x indicates the bacteria was not found.

have the potential for the fabrication of multifunctional scaffolds in diverse biomedical applications, such as dentistry, tissue engineering, wound healing, etc.

4. Conclusion

This study investigated the synthesis of iron-doped biphasic calcium phosphate nanoparticles (FB) and

incorporated silver into them to create a nanostructured composite (FB_{Ag}). These nanoparticles were characterized using various techniques, which revealed that both silver and nitrate were present in the FB_{Ag} nanoparticles, and as the concentration of $AgNO_3$ in the nanoparticles increases, the particles become more irregular in shape and have a reduced particle size distribution. Additionally, cell culture tests revealed that both FB and FB_{Ag} nanoparticles were compatible with bone marrow-derived cells. These findings suggest that the FB_{Ag} nanoparticles may have potential use in biomedical applications, particularly in tissue engineering, due to their antibacterial activity and biocompatibility. The wide range of structural characteristics among various types of FB_{Ag} allows us to tailor the microstructure, morphology, and functional, antibacterial, and biological features of synthetic materials to create better candidates for biomedical applications.

Acknowledgments

Lei Nie acknowledges the support from the Nanhu Scholars Program for Young Scholars of XYNU. The authors acknowledge the help from Prof. Qiuju Zhou, Miss Zihe Jin, Dr Zongwen Zhang, and Dr Dongli Xu, in the Analysis & Testing Center of XYNU.

Data availability statement

All data that support the findings of this study are included within the article (and any supplementary files).

Conflicts of competing interest

The authors declare no competing financial interest.

Statement of ethics

We confirmed that no animal or human experiments were involved in this paper.

ORCID iDs

Lei Nie https://orcid.org/0000-0002-6175-5883

References

[1] Shavandi A *et al* 2015 *Journal of Biomimetics, Biomaterials and Biomedical Engineering* **25** 98
[2] Nie L *et al* 2020 *Sci. Rep.* **10** 13738
[3] Ratnayake J T B *et al* 2017 *J. Biomed. Mater. Res.* B **105** 1054
[4] Han Y *et al* 2021 *Crystals* **11** 353
[5] Shavandi, A *et al* 2015 *Powder Technol.* **273** 33
[6] Nie L *et al* 2020 *ACS Omega* **5** 10948
[7] Mofakhami S and Salahinejad E 2021 *J. Controlled Release* **338** 527
[8] Nie L *et al* 2012 *J. Nanomater.* **2012** 213549
[9] Khatoon Z *et al* 2018 *Heliyon* **4** e01067
[10] Shavandi A *et al* 2019 *In Functional Polysaccharides for Biomedical Applications* ed S Maiti and S Jana (Woodhead Publishing) 8, p 267
[11] Carol López de D *et al* 2020 *Antimicrobial Resistance* ed M Mihai *et al* (IntechOpen) Ch 5
[12] Luo H *et al* 2022 *Microporous Mesoporous Mater.* **346** 112281
[13] Zhao L *et al* 2018 *Composites* B **153** 387
[14] Padmanabhan V P *et al* 2022 *Antibiotics* **11** 1780
[15] Balogh E *et al* 2018 *Pharmaceuticals* **11** 107
[16] Montufar E B *et al* 2018 *Acta Biomater.* **70** 293
[17] Vahabzadeh S and Bose S 2017 *Ann. Biomed. Eng.* **45** 819
[18] Zhang J *et al* 2022 *Journal of Orthopaedic Translation* **32** 103
[19] Katsumata S-I *et al* 2008 *The Journal of Nutrition* **139** 238
[20] McGillivray G *et al* 2007 *Archives of Disease in Childhood* **92** 1088
[21] Zhang D *et al* 2017 *J. Biomed. Mater. Res.* A **105** 148
[22] Mohamed D S *et al* 2020 *Antibiotics* **9** 181
[23] Dakal T C *et al* 2016 *Frontiers in Microbiology* **7** 1831
[24] Nie L *et al* 2020 *Sci Rep.* **10** 1
[25] Yang N *et al* 2022 *Mater. Lett.* 132478
[26] Zhao Y *et al* 2017 *Sci Rep.* **7** 1
[27] Ressler A 2022 *Polymers* **14**
[28] Soitah T N *et al* 2010 *Sci. Adv. Mater.* **2** 534
[29] Mohammed L J and Omer K M 2020 *Sci. Rep.* **10** 3028
[30] Zhang H *et al* 2011 *Biomaterials* **32** 1906
[31] Li J *et al* 2010 *Nanoscale Res. Lett.* **5** 1063
[32] Vinoth Kumar K C *et al* 2021 *Saudi Journal of Biological Sciences* **28** 840
[33] Rao D V *et al* 2017 *Mater. Sci. Eng.* C **74** 207
[34] Yedekçi B *et al* 2021 *J. Mech. Behav. Biomed. Mater.* **115** 104230
[35] Madhukumar K *et al* 2007 *Bull. Mater. Sci.* **30** 527
[36] Lanje A S *et al* 2010 *J. Chem. Pharm. Res.* **2** 478
[37] Yang N *et al* 2022 *Mater. Lett.* **322** 132478
[38] He L *et al* 2019 *Ceram. Int.* **45** 13787
[39] Carofiglio M *et al* 2021 *Nanomaterials* **11** 2628
[40] Kaplan A and Kutlu H M J 2020 *Asian Pacific Journal of Cancer Biology.* **5** 49
[41] Li Y *et al* 2017 *Arch. Toxicol.* **91** 509
[42] Hidalgo E and Domínguez C 1998 *Toxicol. Lett.* **98** 169
[43] Balouiri M *et al* 2016 *Journal of Pharmaceutical Analysis* **6** 71
[44] Kim J S *et al* 2007 *Nanomed. Nanotechnol. Biol. Med.* **3** 95
[45] Mijnendonckx K *et al* 2013 *BioMetals* **26** 609
[46] Song Z *et al* 2019 *Mater. Sci. Eng.* C **99** 255–63